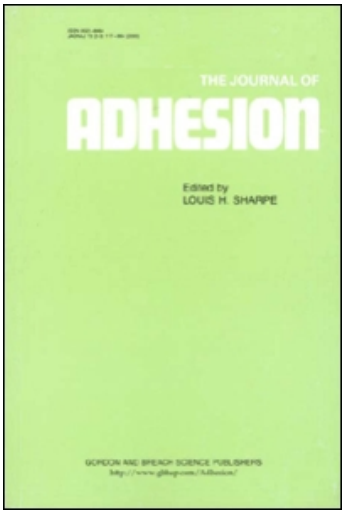

The Journal of Adhesion
Publication details, including instructions for authors and subscription information:
http://www.informaworld.com/smpp/title~content=t713453635

Determination of Residual Stress in Coatings by a Membrane Deflection Technique

Robert M. Jennings[ab]; Jeffrey F. Taylor[ac]; Richard J. Farris[a]
[a] Department of Polymer Science and Engineering, University of Massachusetts, Amherst, MA [b] 3M Center, St. Paul, MN, USA [c] Research Labs, Eastman Kodak Company, Rochester, NY, USA

To cite this Article Jennings, Robert M. , Taylor, Jeffrey F. and Farris, Richard J.(1995) 'Determination of Residual Stress in Coatings by a Membrane Deflection Technique', The Journal of Adhesion, 49: 1, 57 — 74
To link to this Article: DOI: 10.1080/00218469508009977
URL: http://dx.doi.org/10.1080/00218469508009977

J. Adhesion, 1995, Vol. 49, pp. 57–74
Reprints available directly from the publisher
Photocopying permitted by license only

Determination of Residual Stress in Coatings by a Membrane Deflection Technique

ROBERT M. JENNINGS*, JEFFREY F. TAYLOR** and RICHARD J. FARRIS

Department of Polymer Science and Engineering,
University of Massachusetts, Amherst, MA 01003, USA

(Received April 21, 1994; in final form October 28, 1994)

A membrane deflection technique has been developed to measure the isotropic residual stress in biaxially-constrained coatings. The technique has been demonstrated on various materials, including polyimide, latex rubber and photoresist coatings. Stress values obtained from membrane deflection compared well with results obtained from time-averaged vibrational holographic interferometry except for values obtained from samples where rigidity effects were found to be important. A criterion based on the thickness, rigidity, stress and sample radius is also discussed, establishing the applicability of the technique to samples of low rigidity.

KEY WORDS: residual stress; residual stress measurement; membranes; coatings; polyimides; photoresists

1. INTRODUCTION

Residual stress is a key driving force for failure in organic coatings. Most organic coatings develop in-plane residual stresses as a result of changes in temperature, solvent content and/or chemistry during processing under constrained conditions. In many cases these stresses are significant and often lead directly to delamination or fracture of the coating. As a result, in order to understand fully the mechanisms of failure in a particular coating it is important to know the magnitude of the residual stress in the coating.

Various techniques can be used to determine residual stresses in thin films without prior knowledge of the constitutive properties of the coating material. Each of the techniques has various advantages and disadvantages depending on the system one is studying and on the amount of investment one is willing to make. The most widely accepted technique is based on the bending of an underlying substrate.[1] This technique is carried out by applying a coating to a thin, metallic or ceramic substrate. When the coating is cured, the stress developed in the coating will result in bending of the substrate. By knowing the deflection and the bending rigidity of the substrate, the residual stress may be calculated. This technique is versatile and is amenable to application at different temperatures and under many different environments. However,

* Present Address: 3M Center, Bldg. 201-1W-28, St. Paul, MN 55144-1000, USA
** Present Address: Eastman Kodak Company, Research Labs, Rochester, NY 14650-2116, USA

one of the main disadvantages of this technique is that the bending displacements must be comparable with the thickness of the coating. Although these displacements usually can be measured through the use of strain gages or optical techniques, the range of stresses measurable by this technique for a given substrate can be limited.

Another class of stress measurement techniques utilizes the physics of membranes. In these techniques, the substrate is removed from the coating in a geometrically-defined region while maintaining the dimensional constraints on the sample, thus turning the coating into a drum head. Since the coating and substrate do not mechanically interact away from the edges, the original state of stress in the coating is not affected by the removal of the substrate.[2] Although this paper will describe only one technique of substrate removal for sample preparation, many other techniques have been shown to be equally useful.[3–8]

The state of stress in the constrained membrane can be measured by using a few different techniques.[3–10] One of these techniques which has proven to be successful is vibrational time average holographic interferometry.[3–6] The basic principle behind this technique is to find the resonant frequencies and modes of vibration of the membrane that can then be related back to the state of stress with only knowledge of the mass density of the membrane material. This is accomplished by combining the membrane vibration theory with holographic interferometry. This combination is especially powerful since it enables one to determine the entire state of stress in the membrane. The technique can also be applied to membranes under anisotropic stresses and recently the technique has been modified to allow measurements on rigid materials as well.[6] One of the disadvantages of this technique has been that measurements require a vacuum or low density gaseous atmosphere to reduce the damping effect of the surrounding medium during vibration.[5] Therefore, measuring coating stresses in dense gaseous or liquid environments is difficult and requires mathematical corrections. The apparatus required for this technique is also involved and relatively expensive.

If one is reasonably sure that they are dealing with isotropic stresses, another approach is the blister technique whereby a pressure gradient is applied across the membrane and the residual stress is determined by measuring the resulting membrane deflection.[7–10] Knowledge of the sample material properties is not required and the technique is more amenable to application under different temperatures and environments than vibrational techniques. This technique has been shown to be successful for the measurement of residual stresses in metallic and polymeric thin films and it has frequently been used in the measurement of coating adhesion as well.[9,10] However, when dealing with thin organic coatings, measurement of the membrane displacements requires the use of optical techniques and it has been our experience that the apparatus also needs to be isolated from environmental pressure changes (such as closing doors and air conditioners) due to the small differential pressures often involved in the measurement.

In this paper, we will present yet another residual stress measurement similar in concept to the blister test described above. In this technique, a flat circular probe of radius, a, pushes in the center of a constrained circular membrane with a radius, b, as shown in Figure 1. If the bending rigidity of the sample is small then there are no bending stresses associated with the deflection and the restoring force on the probe is a

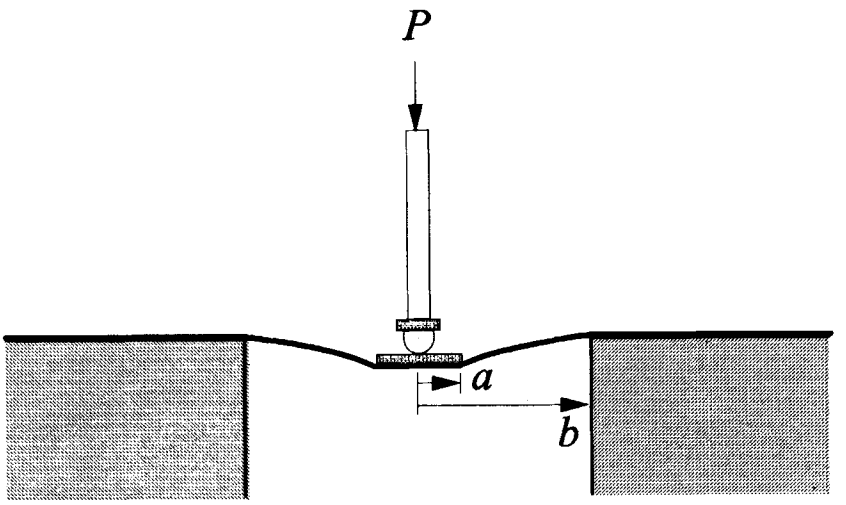

FIGURE 1 Schematic of membrane deflection technique.

function of only the residual stress in the membrane. The residual stress can be determined from knowledge of the load and the resulting probe displacement. The advantages of this technique are: (i) no knowledge of material properties is required (once non-rigidity is assured), (ii) measurements can be made with relative ease using standard equipment, and (iii) utilization in the presence of various environments, *e.g.*, solvents, humidities, or various temperatures, is possible.

THEORY

A force balance performed at the edge of the probe (Fig. 2) reveals that the restoring force, p, is related to the stress in the membrane, σ, the thickness, t, and the angle of the deflected membrane at the probe edge with respect to the probe surface, θ:

$$P = 2\pi a t \sigma \sin(\theta). \tag{1}$$

If θ is small then one can make the approximation: $\sin(\theta) \approx -u'_a = -\lim_{r \downarrow a}(du/dr)$, where r is the radial position in the membrane and u is the out-of-plane deflection of the membrane at r. Substituting into equation (1) and rearranging one finds:

$$\sigma = -\frac{P}{2\pi a t u'_a}. \tag{2}$$

The term, u'_a, can be found using the membrane equation which in its general form (with zero rigidity and excluding momentum effects) can be expressed as:

$$\sigma t \nabla^2 u = \sigma t \left(\frac{\partial^2 u}{\partial r^2} + \frac{1}{r}\frac{\partial u}{\partial r} + \frac{1}{r^2}\frac{\partial^2 u}{\partial \theta^2} \right) = q(r, \theta) \tag{3}$$

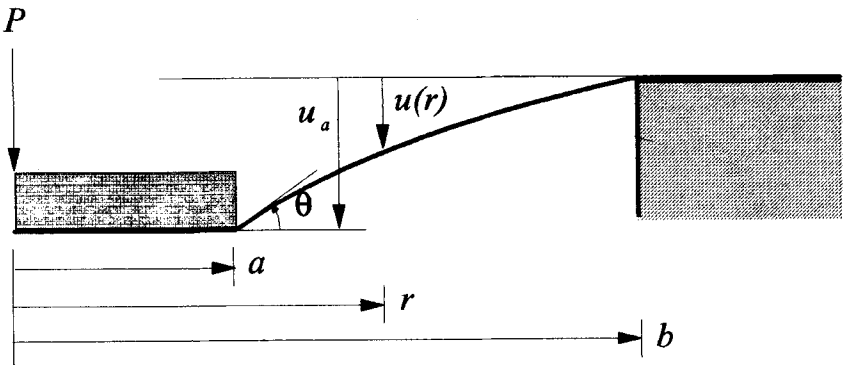

FIGURE 2 Close in schematic of probe edge.

where r and θ are the radial and angular coordinates and q is related to the transverse load on the membrane. In the case of a circular symmetric probe pushing into the center of a circular membrane the load is supported at the outer circumference of the probe. Thus, q is defined as:

$$q(r) = \begin{cases} 0 & r \neq a \\ \dfrac{P}{2\pi a} & r = a \end{cases} \tag{4}$$

and equation (3) reduces to:

$$\frac{\partial^2 u}{\partial r^2} + \frac{1}{r}\frac{\partial u}{\partial r} = 0 \quad (r \neq a). \tag{5}$$

Applying the boundary conditions, $u(a) = u_a$ and $u(b) = 0$, one finds the displacement profile and the slope of the displacement profile to be:

$$u(r) = u_a \frac{\ln(r/b)}{\ln(a/b)} \quad \text{and} \quad u' = \frac{du}{dr} = \begin{cases} \dfrac{u_a}{r\ln(a/b)} & r \geq a \\ 0 & r \leq a. \end{cases} \tag{6}$$

Since bending rigidity is ignored:

$$u'_a = \lim_{r \downarrow a} \frac{du}{dr} = \frac{u_a}{a\ln(a/b)}. \tag{7}$$

Substituting equation (7) into equation (2) the following equation is obtained:

$$\sigma = -\frac{P}{2\pi t u_a}\ln(a/b). \tag{8}$$

The stress in the membrane can easily be determined by measuring the load, P, resulting from a given probe deflection, u_a, or by taking the slope of the load *versus* deflection profile for a number of different deflections.

EXPERIMENTAL

I. Sample Preparation

The techniques used to prepare constrained membrane samples in this study are identical to those presented by Maden and Farris.[3] PMDA-ODA polyimide coatings were prepared by both thermal and chemical curing techniques. Thermally-cured polymide films were prepared by spin coating 15 wt% polyamic acid solutions in N,N'-dimethylacetamide on to tin-coated steel substrates followed by curing at 200°C in a vacuum hot plate oven for 1 hour. Chemically-cured polyimide films were prepared by mixing in stoichiometric amounts of acetic anhydride and β-picoline into the polyamic acid solution prior to spin coating. After the solution was centrifuged for one minute to eliminate air bubbles, it was spin cast and subjected to the same thermal treatment as the thermally-cured coatings.

Photoresist coatings were prepared by laminating a dry film polyacrylate photoresist to tin-coated steel substrates. The coatings were exposed to ultraviolet light by an ultraviolet curing oven supplied by UV Process Supply Inc. The oven was equipped with a D-bulb, medium-pressure, mercury arc lamp with an intensity of 300 watts per inch (118 watts per cm) (exposure dosage: 0.25 J/cm^2). Samples were developed with an aqueous Na_2CO_3 solution (1 wt% $Na_2CO_3 \cdot H_2O$) for 3 minutes followed by rinsing with water. The coatings experienced an ultraviolet cure, dosage of 4 J/cm^2, followed by a thermal cure at 150°C for 1 hour in a ventilated oven.

Constrained membranes were made from the polyimide and photoresist coatings by adhering flat, steel washers (40 mm ID, 75 mm OD) to the coatings with "2-ton" epoxy adhesive, then placing the entire assemblies into a small bath of mercury. The tin coating amalgamates with the mercury releasing the polymeric coatings from the substrate creating drumhead-like membranes constrained by the steel washers. Since tin melts at 232°C, samples prepared on tin-coated steel substrates are limited to thermal treatments less than 220°C. Samples requiring higher thermal treatment may be prepared on silver-coated substrates. A schematic of the sample preparation is shown in Figure 3.

Rubber membrane samples were made by simply biaxially stretching a latex rubber film to different draw ratios then adhering them to the steel washers with Super Glue^{TM}.

II. Stress Measurement

Measurements in this study were made on two different instruments: an Instron^{TM} hydraulic tensile tester and a Dynastat^{TM} dynamic mechanical tester. These instruments provided the possibility of performing measurements at sub-ambient as well as high-temperature environmental conditions. In both cases, simple fixtures were made to hold membrane samples in place on the cross-heads and probes were attached directly to the load cells. A probe consists of a threaded 1/8-inch (3.2 mm) steel rod with a 2 mm diameter steel ball bearing attached to the end. The bearing contacts the center of a 4 mm diameter disk that rests in the center of the 40 mm diameter membrane sample as shown in Figure 4. The rounded probe in contact with a flat disk allows for correction of any asymmetry in the probe.

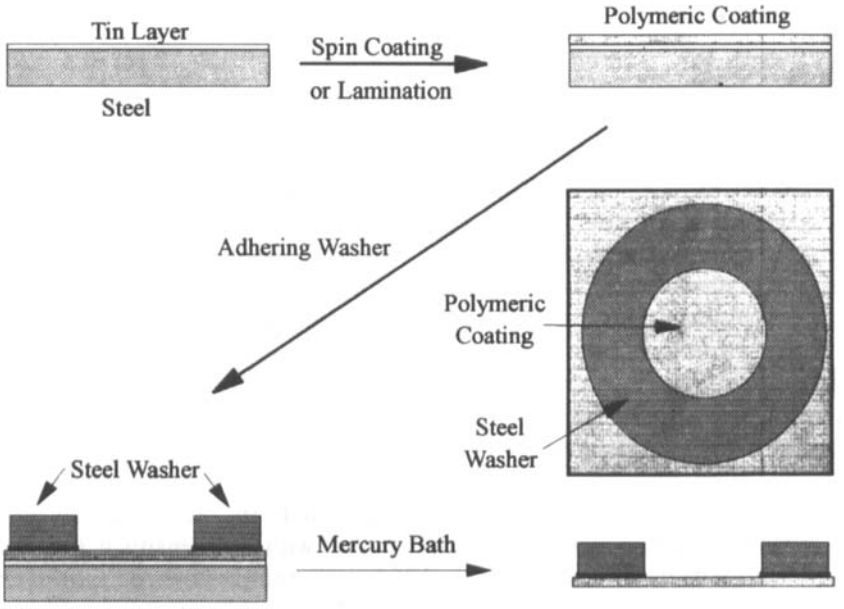

FIGURE 3 Schematic of sample preparation process.

The most accurate method of determining the stress was to push the probe into the sample at a constant rate, then measure the slope of the resulting load *versus* deflection profile. The raw data for a few typical coatings are presented in Figure 5. Using this technique only a relative value of the displacement is needed, eliminating the need for determining zero displacement. In most cases, the measurements were begun with the probe just contacting the membrane with a slightly positive load. A "saw-tooth" shaped displacement input was applied to the samples with periods between 10 and 45 seconds and typical maximum deflections between 10 and 40 μm to insure that in-lane stress changes due to the deflection were insignificant. Since in-plane stresses resulting from the deflection are small, the measurement is independent of the rate of deflection. As observed in Figure 5, the restoring force on the probe was found to be proportional to the deflection and the maximum loads measured typically ranged between 3 and 40 grams depending on the stresses and sample thickness. All measurements were determined from an average of three cycles.

Stress measurements from membrane deflection were compared with measurements using holographic interferometry in order to verify the accuracy of the deflection technique. Both measurements were made on the same samples. The resonant frequencies of the stressed membranes were found by vibrating the sample at different frequencies under vacuum. The frequencies of the various samples are identified by superimposing the holographic image of a vibrating sample over a stationary sample image, thus producing interference patterns indicative of the mode of sample vibration. For a circular membrane, the modes of vibration are dictated by the zeroes of Bessel functions and frequencies at which the modes occur determine the stress in the

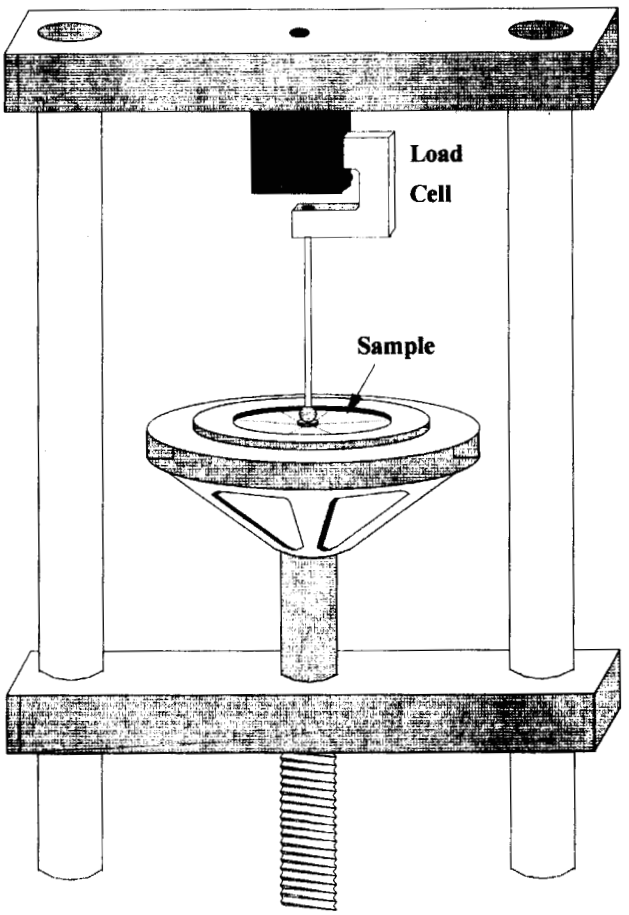

FIGURE 4 Schematic of membrane deflection fixture.

membrane through the simple relation:

$$\sigma = \frac{\rho \omega_{nl}^2 b^2}{Z_{nl}^2} \tag{9}$$

where ρ is the membrane density, ω is the measured frequency of vibration, b is the sample radius and Z_{nl} is the lth zero of the corresponding nth order Bessel function. The reader is referred to references 3–5 for a more detailed description of the holographic interferometry technique. The accuracy of the holographic stress measurement is estimated to be on the order of $\pm$ 10% and we have found the measurements to be quantitatively consistent with uniaxial stress measurements made on both polyimide and photoresist films.[11,12] For the purpose of this discussion we will treat the results of the holographic stress measurements as the true magnitudes of biaxial stress in the samples tested.

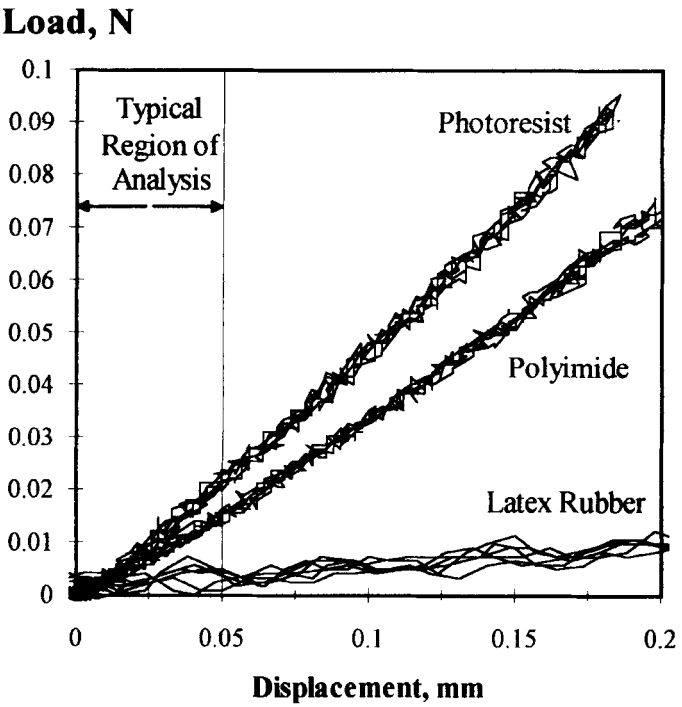

FIGURE 5 Typical load/displacement responses for a few typical coatings.

RESULTS

The results of measurements made on various coatings using both the membrane deflection and holography techniques are shown in Table I. Measurement results from both membrane deflection and holography were found to be self-consistent with typical standard deviations of less than $\pm$ 5%. Stress measurement results from the membrane deflection technique were very consistent with those obtained from holography on the polyimide, polyurethane and latex rubber membranes. However, stresses measured on the photoresist samples using membrane deflection were consistently 20 to 50% lower than stresses measured by holography on the same samples. Comparison of the measurement results with the modulus and thickness of the samples (also shown in Table I) reveals that the deviations occur in samples with both high moduli and large thickness suggesting that the zero-rigidity assumption behind this technique is violated in these samples. The 50% lower apparent stress values was a recurring result in many of the samples tested with moderate rigidity using the deflection technique.

This conclusion was surprising since the rigidity corrections for these samples in the holography technique are very small.[6] In addition, the presence of large rigidity in samples tends to increase the resonant vibration frequencies of those samples, resulting in apparent stress measurements from the holographic technique higher than the true stresses in the samples. Based on this evidence, the presence of sample rigidity was expected to cause a slightly higher apparent stress measurement using the deflection technique as well.

TABLE I
Comparison of the residual stress determined by membrane deflection and vibrational holographic interferometry.

Sample	Modulus (MPa)	Thickness (μm)	Deflection Stress (MPa)	Holography Stress[True Stress] (MPa)	Bending Rigidity ($Pa\,m^3$)	k (m^{-1})
Latex Rubber: elongation ratio = 1.25	10	85	0.45 ± 0.00	0.42 ± 0.00	6.82×10^{-7}	14450
Latex Rubber: elongation ratio = 1.43	10	85	0.92 ± 0.00	0.98 ± 0.00	6.82×10^{-7}	22100
Thermally-Cured Polyimide	3000	11.4	19.8 ± 0.03	19.8 ± 0.03	4.07×10^{-7}	47100
Chemically-Cured Polyimide	3000	7.5	15.2 ± 0.75	15.6 ± 0.11	1.10×10^{-7}	65000
Polyurethane (50% hard segments)	140	115	1.12 ± 0.01	1.28 ± 0.04	2.36×10^{-5}	4995
Polyurethane (40% hard segments)	70	80	0.42 ± 0.02	0.45 ± 0.02	3.18×10^{-6}	6750
Polyurethane (30% hard segments)	14	80	0.35 ± 0.03	0.33 ± 0.01	6.37×10^{-7}	12900
Low Stressed Photoresists	1750	86.2	2.36 ± 0.09	4.47 ± 0.22	1.03×10^{-4}	3870
High Stressed Photoresists	2000	92.5	6.47 ± 0.25	9.69 ± 0.48	1.45×10^{-4}	4975

Rigidity Effects

In order to explain this discrepancy and to determine the conditions under which sample rigidity is important, it was necessary to model further the deflection technique including both in-plane stress and rigidity effects. The force balance for the symmetric bending of a rigid plate with an in-plane stress is given by:[13]

$$P = -2\pi at\sigma u'_a + 2\pi aD\left[u'''_a + \frac{1}{a}u''_a - \frac{1}{a^2}u'_a\right] \tag{10}$$

where u, t, σ and P have been defined previously and D is the bending rigidity of the sample defined as:

$$D = \frac{Et^3}{12(1-\nu^2)} \tag{11}$$

for a circular sample with a tensile modulus E and Poisson's ratio ν. Note that equation (10) is similar to the force balance used earlier in equation (1) with an added term for rigidity. Once again, the deflection profile must be found to provide the derivatives of the deflection profile at the probe edge required in equation (10).

The deflection profile can be found by solving a more general form of the membrane equation (equation (3)) in which a term for bending rigidity is added:

$$D\nabla^4 u - \sigma t\nabla^2 u = q(r,\theta) \tag{12}$$

where $q(r,\theta)$ is once again defined as:

$$q(r) = \begin{cases} 0 & r \neq a \\ \dfrac{P}{2\pi a} & r = a \end{cases}$$

The solution to equation (12) is rather complicated and as a result is shown in the Appendix. In addition to the displacement boundary conditions used in the solution to equation (3) it is also necessary to impose three more boundary conditions. The first boundary condition is a clamped condition at the outer boundary resulting in $u'(b) = 0$. The other two are a statement of continuity at the probe edge which is met by imposing the condition: $\lim_{r\downarrow a} du/dr = \lim_{r\uparrow a} du/dr$ and $\lim_{r\downarrow a} d^2u/dr^2 = \lim_{r\uparrow a} d^2u/dr^2$. Note that these boundary conditions disappear in the limit of zero rigidity. In fact, the reader will recall that the solution to the membrane equation has a discontinuity in the slope of the deflection profile at the probe edge. This is a clue to the measured discrepancies noted above.

The resulting solution for the deflection profile of a rigid plate under in-plane tension is:

$$0 \le r \le a: \quad u(r) = u_a + A_1[I_0(R) - I_0(A)]$$

$$a \le r \le b: \quad u(r) = u_a\frac{\ln(r/b)}{\ln(a/b)} + B_1\left[I_0(R) - I_0(B) - [I_0(A) - I_0(B)] - I_0(B)\frac{\ln(r/b)}{\ln(a/b)}\right]$$

$$+ B_2\left[K_0(R) - K_0(B) - [K_0(R) - K_0(B)]\frac{\ln(r/b)}{\ln(a/b)}\right] \tag{13}$$

where A_1, B_1 and B_2 are constants defined in the Appendix, $I_n(R)$ and $K_n(R)$ are the nth order modified Bessel functions of the first and second kind, A, B and R are dimensionless quantities defined, respectively, as: $R = rk$, $A = ak$ and $B = bk$ and k is defined as:

$$k = \left(\frac{t\sigma}{D}\right)^{1/2}. \tag{14}$$

The term k characterizes the relative amount of rigidity in the sample. When $k = 0$, the stress term in equation (10) disappears and equation (13) reduces to the solution of the symmetric bending of a rigid circular plate given by:

$$0 \le r \le a: \quad u(r) = u_a \frac{(b^2 + r^2)(b^2 - a^2) + 2(a^2 + r^2)b^2 \ln(a/b)}{b^4 - a^4 + 4a^2b^2 \ln(a/b)}$$

$$a \le r \le b: \quad u(r) = u_a \frac{(b^2 - r^2)(b^2 + a^2) + 2(a^2 + r^2)b^2 \ln(r/b)}{b^4 - a^4 + 4a^2b^2 \ln(a/b)} \tag{15}$$

As k approaches infinity the rigidity term in equation (12) disappears and equation (13) describes the deflection profile of a membrane given by equation (6). To demonstrate this more fully, the calculated deflection profiles and first derivatives for the membrane, plate and combination solutions are shown in Figure 6 for a range of k values. The profiles are calculated for $a = 2\,\text{mm}$, $b = 20\,\text{mm}$ and $u_a = 1\,\mu\text{m}$. The range of k values can be generated by varying σ, t or D with equivalent effects on the profile. Note that for most values of k the first derivative of the deflection profile is continuous over the entire radius of the sample. However, as k becomes large a discontinuity develops at the probe edge becoming consistent with the membrane solution.

In order to see the effects of the deflection profile on the restoring force, P, it is helpful to divide the restoring force into a stress component, P_s, and a rigidity component, P_r. The stress component is defined exactly the same way as it was for the force balance in the membrane solution and the rigidity component is defined as the extra term added to the force balance in equation (10):

$$P_s = -2\pi a t \sigma u'_a$$

$$P_r = 2\pi a D \left[u'''_a + \frac{1}{a} u''_a - \frac{1}{a^2} u'_a \right] \tag{16}$$

where: $P = P_s + P_r$. A plot of these two components is shown in Figure 7 as a function of k together with calculated restoring forces for the membrane and plate solutions. These curves were calculated using the same sample dimensions and deflection used to calculate the profiles in Figure (6). When varying k for these calculations the stress and thickness were held constant at 10 MPa and 100 μm, respectively, while only the rigidity was varied.

Both plots in Figure 7 indicate a transition occurring in the region of $k \sim 100$ to $1000\,\text{m}^{-1}$. For small values of k the rigidity component of the restoring force matches the restoring force for the plate solution. The rigidity component is also much larger than the stress component, indicating that the total restoring force for the exact solution approaches the restoring force for the plate solution under these conditions. However, for large values of k the stress component of the restoring force does not

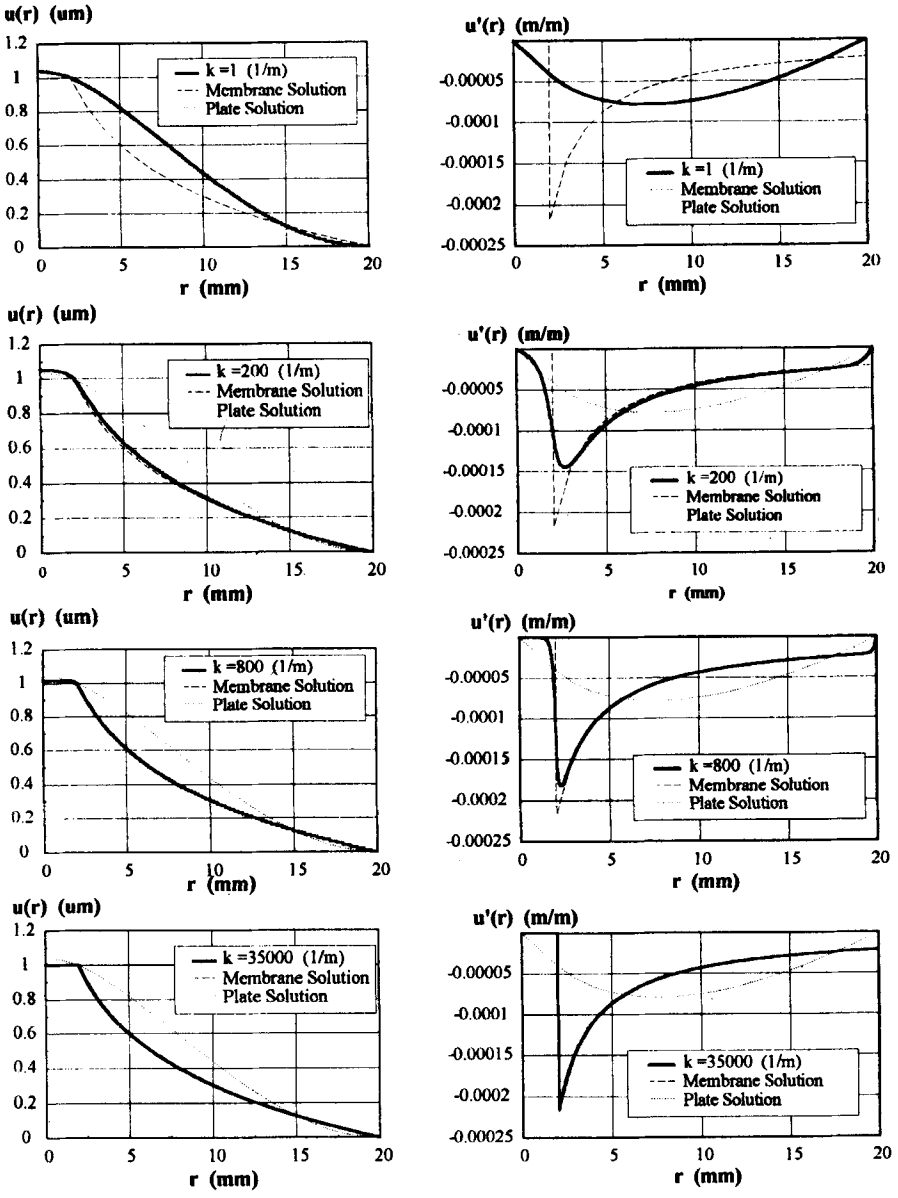

FIGURE 6 Deflection profile and 1st derivative for membrane, plate and exact solutions for $a = 2\,\text{mm}$, $b = 20\,\text{mm}$ and $u_a = 1\,\mu\text{m}$.

approach the restoring force for the membrane solution but approaches a value of exactly one-half of the restoring force predicted by the membrane solution. In addition, the rigidity component of the restoring force does not continue to decrease with increasing k but also approaches a value of exactly one-half of the restoring force for the membrane solution.

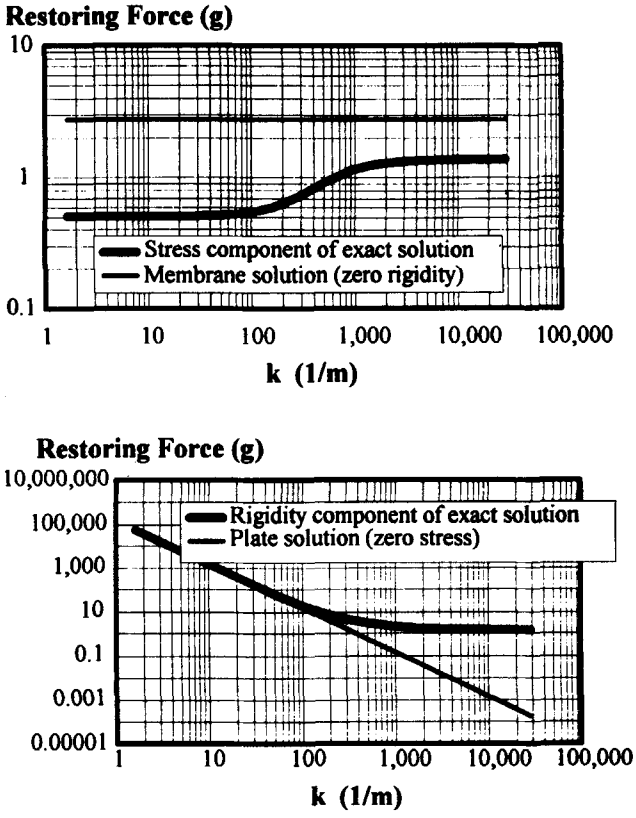

FIGURE 7 Plots of calculated restoring force *versus* k for a 1 μm deflection of a sample with a radius of 20 mm, stress 10 MPa and thickness 100 μm using a probe with radius 2 mm.

This behavior at large values of k can also be verified analytically by using asymptotic approximations for the Bessel functions for large arguments:[14]

$$I_n(R) \approx (2\pi R)^{-1/2}\exp(R)$$

$$K_n(R) \approx \pi(2\pi R)^{-1/2}\exp(-R). \tag{17}$$

Using these approximations, the restoring force components in equation (16) reduce to:

$$P_s = -\frac{2\pi\sigma t u_a AB}{2AB\ln(a/b) - 2A - B}$$

$$P_r = -\frac{2\pi D u_a A^3 B}{a^2[2AB\ln(a/b) - 2A - B]}. \tag{18}$$

When we substitute the definitions for A and B and let $D = 0$, the components of the restoring force reduce further to:

$$P_s = P_r = -\frac{\pi\sigma t u_a}{\ln(a/b)}. \tag{19}$$

Comparison of the stress component of the restoring force to the load predicted by the membrane (equation (8)) shows the two results to differ by exactly a factor of two. If one looks at the deflection profile at the probe edge one finds that the first derivative of the profile in the limit of zero rigidty is also one-half the value obtained in the membrane solution (equation (7)):

$$u'_a = \frac{P_s}{2\pi\sigma t} = \frac{1}{2}\frac{u_a}{ln(a/b)} \tag{20}$$

To make things even more puzzling, when the stress and rigidity components of the restoring force are added together in the limit of zero rigidity, one finds the same relationship between the total restoring force and probe deflection as found in the membrane solution (equation (8)), even though the calculations of the first derivatives of the deflection profiles in the two cases differ by a factor of two!

The ambiguity in the deflection profile can easily be understood by inspection of the deflection profiles shown in Figure (6). In the limit of zero rigidity, the maximum slope in the deflection profile occurs at the probe edge. A discontinuity exists at the probe edge as well. Just inside the probe radius, the slope of the deflection profile is zero while just outside the probe radius the slope of the deflection profile takes on a finite negative value. However, when even a small amount of rigidity is present, the maximum in the slope of the deflection profile moves slightly away from the probe edge and the slope of the deflection profile at the probe edge drops to a value of one-half of the slope maximum (the average value of the slopes on each side of the probe edge). Even though the deflection profile can be accurately described by membrane theory everywhere in the sample, membrane theory fails at the probe edge when the membrane possesses even a small bending rigidity. This behavior does not occur in time-averaged holographic interferometry measurements. The question that remains is how much rigidity may be present in membrane samples before large errors are introduced into the membrane deflection measurements?

In order to answer this question, k values were calculated for the samples listed in Table I. These values are also listed in the table and a plot of the measured stress divided the true stress (measured by holography) is shown as a function of k in Figure 8. The plot demonstrates that the rigidity effects on the stress measurement start to become important for $k < \sim 10000\,\mathrm{m}^{-1}$. Measurements on samples with $k > 10000\,\mathrm{m}^{-1}$ agree with the true stress values to within $\pm 10\%$.

Note that the results shown in Table I were obtained using a probe radius of 2 mm and a sample radius of 20 mm, resulting in a probe-to-sample radius ratio of: $a/b = 0.1$. In order to see the effects of the probe and sample radius on the measurement, a number of measurements were made using different probe radii on the two photoresist samples. The results of these measurements, shown in Figure 9, demonstrate

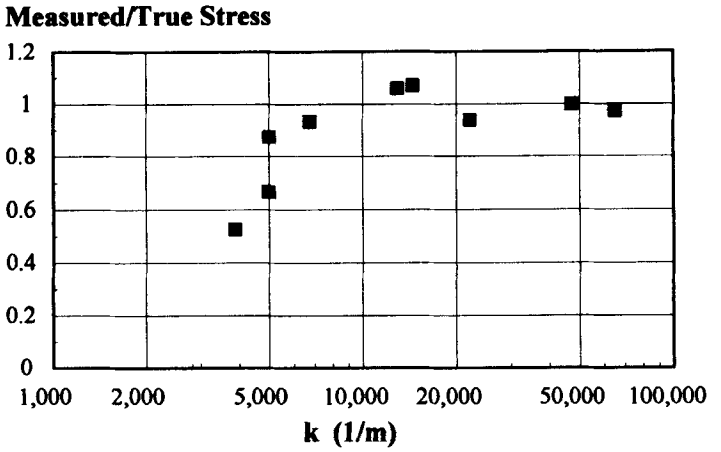

FIGURE 8 Plot of measured stress (by membrane deflection) divided by true stress (measured by holography) *versus* k.

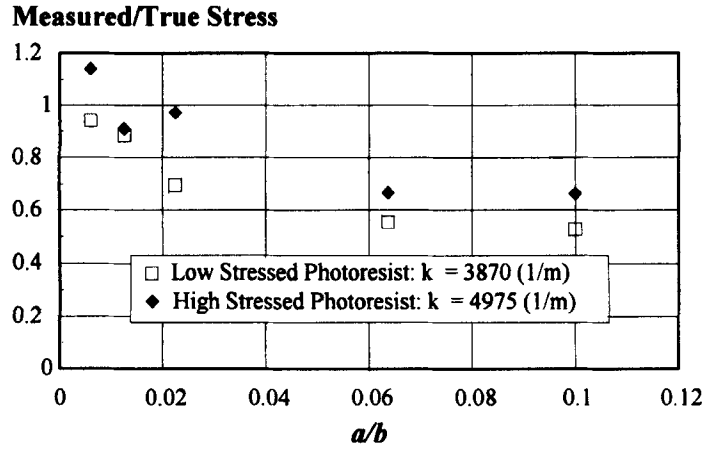

FIGURE 9 Plot of measured stress (by membrane deflection) divided by true stress (measured by holography) *versus* probe to sample radius ratio (*a*/*b*).

that as probes of smaller radii are used, the stresses measured by the membrane deflection technique become closer to those measured by holography. Thus, the use of smaller diameter probes was found to decrease the amount of error resulting from sample rigidity in the membrane deflection measurements. However, it was also found that, when making measurements on thin samples with very low rigidity ($k > 10000\,\mathrm{m}^{-1}$), the larger diameter probes were more convenient to use and resulted in less signal noise due to the larger loads imposed on the sample for a given deflection.

CONCLUSIONS

The membrane deflection technique is a relatively simple and straight-forward technique for measuring isotropic, biaxial stresses in polymeric coatings. Measurements made using this technique were found to agree very well with measurements made using time-averaged holographic interferometry for non-rigid samples but were found to be inconsistent for samples with moderate rigidity. A rigidity criterion, k, based on the rigidity, thickness and residual stress in the sample, was also introduced to determine quantitatively when sample rigidity is important for the deflection technique. Measurement results indicate that samples with $k > \sim 10000\,\mathrm{m}^{-1}$ may be tested successfully with the membrane deflection technique with a sample-to-probe diameter ratio of 0.1. It was found that the technique can be extended to samples with lower k values smaller probe diameters.

Establishing of this technique is easily done on tensile testers capable of resolving loads on the order of grams and displacements on the order of micrometers. In addition, this technique is versatile in that the ambient environment possible for testing is unlimited. The presence of various temperatures, humidities or solvents do not affect the stress measurements. A simple and versatile technique has been needed, and in many application this membrane deflection technique will be highly useful.

References

1. K. L. Chopra, *Thin Film Phenomena* (McGraw-Hill, New York, 1969), Chap. 5, p. 256.
2. B. J. Aleck, *J. App. Mechanics*, **16** (2), 118 (1949).
3. M. A. Maden and R. J. Farris, *Mat. Res. Soc. Symp. Proc.*, **154**, 143 (1989).
4. A. Jagota, S. Mazur and R. J. Farris, *Mat. Res. Soc. Symp. Proc.*, **188**, 35 (1990).
5. M. A. Maden, K. Tong, R. J. Farris, *Mat. Res. Soc. Symp. Proc.*, **188**, 29 (1990).
6. Q. K. Tong, *Characterization of Processing Stresses and Structure-Property Relationships of a Polyacrylate Photoresist*, Ph.D. Thesis, University of Massachusetts, Amherst, MA (1993).
7. E. I. Bromley, J. N. Randall, D. C. Flanders and R. W. Mountain, *J. Vac. Sci. Technol.*, **B1** (4), 1364 (1983).
8. M. G. Allen, M. Mehregany, R. T. Howe and S. D. Senturia, *Appl. Phys. Lett.*, **51** (4), 241 (1987).
9. H. Dannenburg, *J. Appl. Polym. Sci.*, **5** (14), 125 (1961).
10. M. L. Williams, *J. Appl. Polym. Sci.*, **13**, 29 (1969).
11. R. M. Jennings, *An Investigation of the Effects of Curing Conditions on the Residual Stress and Dimensional Stability in Polyimide Films*, Ph.D. Thesis, University of Massachusetts, Amherst, MA (1993).
12. J. F. Taylor, *An Experimental Evaluation of the State of Stress and Mechanical Performance of a Polyacrylate Photoresist Coating*, Ph.D. Thesis, University of Massachusetts, Amherst, MA (1993).
13. S. Timoshenko and S. Woinowsky-Krieger, *Theory of Plates and Shells*, 2nd Ed., (McGraw-Hill, New York, 1959).
14. W. H. Press, B. P. Flannery, S. A. Teukolsky and W. T. Vetterling, *Numerical Recipes, The Art of Scientific Computing* (Cambridge University Press, New York, 1986).
15. D. O. Pettersson, *Acta Polytechnica, Stockholm*, no. 138, (1954).

APPENDIX: Exact Solution for Deflection of a Rigid Plate under In-Plane Stress

The general solution to equation (12) is:

$$u(r) = A_1 I_0(R) + A_2 K_0(R) + A_3 \ln r + A_4 \tag{A1}$$

where A_i are constants, $I_n(R)$ and $K_n(R)$ are the nth order modified Bessel functions of the first and second kind and R is a dimensionless quantity defined as: $R = rk$ and $k = \sqrt{\sigma t/D}$. This solution can be verified using Frobenius method and is very similar to the solution found for the symmetrical bending of a circular plate under lateral compression.[15] In order to apply this solution to the membrane deflection problem it is necessary to break up the membrane surface into two regions: $0 \le r \le a$ and $a \le r \le b$. We will also need to use a separate set of constants to describe the deflection profile in the two regions and as a result equation (A1) will be expressed as:

$$u(r) = A_1 I_0(R) + A_2 K_0(R) + A_3 \ln r + A_4 \quad 0 \le r \le a$$

$$u(r) = B_1 I_0(R) + B_2 K_0(R) + B_3 \ln r + B_4 \quad a \le r \le b. \tag{A2}$$

In the region $0 \le r \le a$, $K_0(R)$ and $\ln r$ are undefined at $r = 0$. Therefore, the constants A_2 and A_3 must be zero and equation A2 reduces to:

$$u(r) = A_1 I_0(R) + A_4 \quad 0 \le r \le a$$

$$u(r) = B_1 I_0(R) + B_2 K_0(R) + B_3 \ln r + B_4 \quad a \le r \le b. \tag{A3}$$

If we apply the same boundary conditions that we applied for the membrane solution ($u(a) = u_a$ and $u(b) = 0$) equation (A3) can be reduced further:

$$u(r) = u_a + A_1[I_0(R) - I_0(A)] \quad 0 \le r \le a \tag{A4a}$$

$$u(r) = u_a \frac{\ln(r/b)}{\ln(a/b)} + B_1\left[I_0(R) - I_0(B) - [I_0(A) - I_0(B)\frac{\ln(r/b)}{\ln(a/b)}\right]$$

$$+ B_2\left[K_0(R) - K_0(B) - [K_0(A) - K_0(B)\frac{\ln(r/b)}{\ln(a/b)}\right] \quad a \le r \le b \tag{A4b}$$

where A and B are defined as : $A = ak$ and $B = bk$.

In order to find the three remaining constant in equation (A4) it is necesssary to apply three more boundary conditions to the system. The boundary conditions are:

$$\left.\frac{du}{dr}\right|_{r=b} = 0, \quad \lim_{r \downarrow a}\frac{du}{dr} = \lim_{r \uparrow a}\frac{du}{dr}, \quad \text{and} \quad \lim_{r \downarrow a}\frac{d^2u}{dr^2} = \lim_{r \uparrow a}\frac{d^2u}{dr^2} \tag{A5}$$

and are a result of clamped conditions of the coating at the outer edge and continuity at the probe edge. The constants A_1, B_1 and B_2 can then be found by setting the first derivative of equation (A4b) equal to zero at $r = b$ and by setting the first and second derivatives of equation (A4a) and (A4b) equal to each other. The three remaining constants then become:

$$A_1 = u_a \frac{1}{C}\{B[I_0(A)K_1(B) + K_0(A)I_1(B)] - A[I_0(A)K_1(A) + K_0(A)I_1(A)]\}$$

$$B_1 = u_a \frac{1}{C}\{BI_0(A)K_1(B) - A[I_0(A)K_1(A) + K_0(A)I_1(A)]\}$$

$$B_2 = u_a \frac{1}{C}BI_0(A)I_1(B) \tag{A6}$$

where:

$$C = ABI_1(B)[I_0(A)K_1(A) + K_0(A)I_1(A)]\ln(a/b)$$
$$- A[I_0(B) - I_0(A)][I_0(A)K_1(A) + K_0(A)I_1(A)]$$
$$+ BI_0(A)\{[K_0(B) - K_0(A)]I_1(B) + [I_0(B) - I_0(A)]K_1(B)\}.$$